CHEMISTRY OF MATERIALS

Article

pubs.acs.org/cm

Single-Crystal Tungsten Oxide Nanosheets: Photochemical Water Oxidation in the Quantum Confinement Regime

Mollie R. Waller,[†] Troy K. Townsend,[†] Jing Zhao,[†] Erwin M. Sabio,[†] Rachel L. Chamousis,[†] Nigel D. Browning,[‡] and Frank E. Osterloh*[,†]

[†]Department of Chemistry and [‡]Department of Chemical Engineering and Materials Science, Department of Molecular and Cellular Biology, University of California, Davis, One Shields Avenue, Davis, California 95616, United States

ABSTRACT: Here we investigate the structure, photophysics, and photocatalytic water splitting properties of single-crystalline WO_3 nanosheets (0.75 nm × 90 ± 38 nm), obtained by exfoliation from $Bi_2W_2O_9$. Upon delamination, the nanosheets undergo a structural change from tetragonal symmetry in the parent material to monoclinic, as confirmed by powder X-ray diffraction and electron microscopy. Diffuse reflectance optical spectra show band gap energies consistent with quantum confinement in nano-WO_3 (E_G = 2.88 eV) and $Bi_2W_2O_9$ (E_G = 2.81 eV), relative to bulk WO_3 (E_G = 2.68 eV). Surface photovoltage measurements on nano-WO_3 films on a F:SnO_2 substrate demonstrate photochemical carrier formation under band gap excitation and irreversible trapping of holes. Photochemical oxygen formation is observed with 50 mg of the material in aqueous $AgNO_3$ and $(NH_4)_2Ce(NO_3)_6$ solutions under full spectrum (>250 nm) or visible only (>400 nm) irradiation. The highest initial O_2 evolution rates (69.7 μmol h^{-1} for bulk and 35.5 μmol h^{-1} for nano-WO_3) are observed under >250 nm illumination in the presence of 8.3 mM $AgNO_3$(aq). Quantum efficiencies (at 375 nm) reach 1.43% and 1.55% for bulk and nano-WO_3, respectively. Electrochemical measurements reveal large water oxidation overpotentials (0.96 V) for both nano- and bulk-WO_3. On the basis of photo-onset measurements, the conduction band edges in nano-/bulk-WO_3 are at +0.11/+0.23 V, respectively. Overall, the data show that the photoelectrochemical water oxidation ability of WO_3 is maintained in 0.75 nm nanocrystal WO_3 sheets, although more energetic photons are required because of the extended band gap.

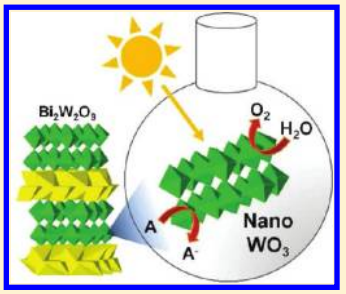

KEYWORDS: *water oxidation, water splitting, photocatalysis, catalysis, WO_3, tungsten oxide, nanosheet, nanocrystal, quantum confinement, solar energy conversion*

INTRODUCTION

Tungsten trioxide crystallizes in the ReO_3 structure type and is an n-type semiconductor with a 2.7 eV band gap. Since the early works by Hodes and separately by Bard, WO_3 has been considered as a promising photoanode material for water oxidation, either as part of a photoelectrochemical cell,[1,2] or as suspended powder in the presence of a chemical bias.[3] Turner recently demonstrated a Tandem cell for overall water splitting that used a WO_3 photoanode in combination with a $GaInP_2$ photoanode.[4] Tandem systems based on suspended WO_3 particles were also developed by Kudo[5,6] and by Domen.[7−10] Under acidic conditions, WO_3 generally shows good stability, but photocurrents and quantum yields are low in comparison with TiO_2.[1] These issues could potentially be addressed by nanoscaling the material, which can reduce kinetic charge transfer limitations and increase the thermodynamic driving force via a quantum size effect.[11,12] For example, enhanced photocatalytic benzene degradation by 1.4 nm WO_3 nanocrystals was recently reported by Tanaka.[13]

Schaak et al. recently showed that single-crystalline, subnanometer thin WO_3 nanosheets can be obtained from the layered compound $Bi_2W_2O_9$. This material consists of $W_2O_7^{(2-)}$ sheets, which are held together by $Bi_2O_2^{2+}$ layers (Figure 1). When $Bi_2W_2O_9$ is treated with 6 M HCl at room temperature, selective etching of $Bi_2O_2^{2+}$ layers occurs, and the WO_3 layers

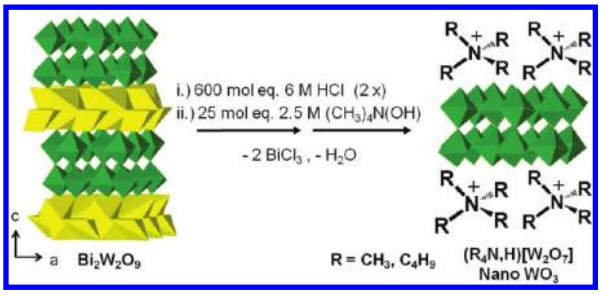

Figure 1. Conversion of $Bi_2W_2O_9$ to give $(R_4N,H)[W_2O_7]$ nanosheets (nano-WO_3) using a method adapted from Schaak et al.[14]

can be stabilized in the presence of tetramethylammonium surfactant.[14] The resulting nanosheets (described as nano-WO_3 in the following) have the formal composition $H_2W_2O_7$. Like in the parent compound, the WO_6 units are stacked in two levels, giving the sheets a thickness of only 0.75 nm, based on crystallography. Here we report for the first time on the optical, photophysical, electrochemical and photochemical water oxidation properties of the WO_3 nanosheets and contrast them with

Received: November 3, 2011
Revised: December 17, 2011
Published: February 16, 2012

bulk-WO_3. We find that nano-WO_3 is similar to bulk-WO_3, except for an extended band gap that results from quantum confinement. These results demonstrate that the basic photochemical water oxidation functionality of WO_3 does not require an extended lattice. It also demonstrates nano-WO_3 could be used as functional replacement for WO_3, for example in the form of ultrathin films.

EXPERIMENTAL SECTION

Materials. Bi_2O_3 (99.9999%), WO_3 (99+%), tetramethylammonium hydroxide (TMA(OH), 25 wt % in water), tetrabutylammonium hydroxide (TBA(OH), 40 wt % in water) and ammonium cerium(IV) nitrate ($(NH_4)_2Ce(NO_3)_6$), 99.5%) were obtained from Acros Organics and used as received. Hydrochloric acid and $AgNO_3$ were obtained from Fischer Scientific and concentrated H_2SO_4 (95−98%) was received from Sigma-Aldrich. Water was purified by a Nanopure II system to a resistivity of >18 MΩ cm.

WO_3 Nanosheets. (adapted from Schaak et al).[14] Stoichiometric amounts of Bi_2O_3 (5.06 g) and WO_3 (4.98 g) were combined and ground to a fine powder with a mortar and pestle. The powder was pressed into pellets and calcined at 800 °C for 16 h. The resulting yellow solid ($Bi_2W_2O_9$, 19.73 g) was again ground to a fine powder and 6.50 g suspended in 710 mL of 6 M HCl (600 mol excess) at RT with stirring. After three days the solid was centrifuged at 3700 rpm for five minutes and the acidic supernatant discarded. The solid was suspended in fresh acid, stirred for three more days, centrifuged off, and washed five times with water before it was dried at 90 °C in an oven overnight to give 3.23 g of yellow solid; 3.19 g of this material ($H_2W_2O_7$) was suspended in 60.57 g of the TMA(OH) solution (25 mol excess) and stirred at room temperature for 21 days. The exfoliated tungstate (nano-WO_3) was separated by centrifugation. The solid was then washed with water to pH ∼6, and dispersed in water for further work up.

Work Up. Dilute TBA(OH)(aq) (0.5 wt %) was added dropwise to pH ∼9 and the solution (approximately 1.5 g material in 50 mL water) was sonicated for 15 min (steps 1i and 1ii in Figure 2). The suspension

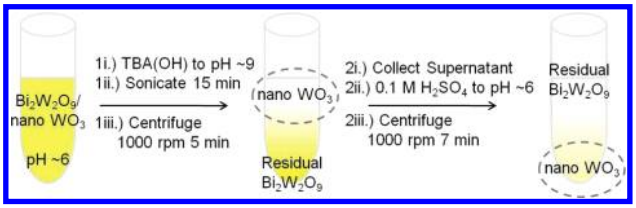

Figure 2. Separation of nano-WO_3 from residual $Bi_2W_2O_9$ material and side products. The final precipitate is suspended in 0.5 wt % TBA(OH) for further studies.

was then centrifuged at 1000 rpm for 5 min and the cloudy, white supernatant collected (steps 1iii and 2i). The yellow precipitate was discarded. To the supernatant was added dropwise dilute $H_2SO_{4(aq)}$ (0.1 M), with stirring, to pH ∼6 (step 2ii). This solution was immediately centrifuged at 1000 rpm for 7 min (step 2iii). The slightly cloudy supernatant was discarded and the white precipitate, well exfoliated tungstate nanosheets (nano-WO_3), was dispersed in 0.5 vol % TBA(OH)(aq) for storage. A final product mass of approximately 70 mg represents an overall yield for the process of approximately 4.5%.

Photocatalytic O_2 Evolution. Irradiation experiments were performed using a 300 W Xe lamp, equipped with a water IR filter and with a 400 nm long-pass filter when necessary. The power received at the flask was ∼390 mW cm^{-2} without and ∼315 mW cm^{-2} with the long-pass filter. Fifty milligrams of the catalyst was suspended in 50 mL of an aqueous solution of the sacrificial electron acceptor (either $AgNO_3$ or $(NH_4)_2Ce(NO_3)_6$ at variable concentration, see Table 1) in a 50 mL quartz flask. After being evacuated and purged with argon three times, the stirred solution was irradiated for 5 h with periodic tests of the gas composition. A Varian gas chromatograph with a Supelco molecular 60/80 sieve 5A column and thermal conductivity detector (TCD) with argon as a carrier gas was used for analysis. For quantum efficiency determinations a 375 nm LED (Roithner Lasertechnik) was used for irradiation of 10 mg of the catalyst in 50 mL of 2.1 mM aqueous $AgNO_3$. For the nano-WO_3 quantum efficiency determination the flux was 2.28×10^{-7} mol photons s^{-1}, based on the measured power (5.40 mW cm^{-2}) of the LED using a GaAsP detector. For the bulk-WO_3 quantum efficiency determination the flux was 1.63×10^{-7} mol photons s^{-1}, based on a measured power of 3.86 mW cm^{-2}. The quantum efficiency was calculated assuming that four photons are necessary for one molecule of O_2.

Electrochemistry. Electrochemical measurements were performed using a three-electrode cell equipped with a Pt counter electrode and SCE reference electrode. A fluorine-doped tin oxide (FTO) coated glass electrode (1.0 cm^2 exposed area) covered by the WO_3 samples served as the working electrode. Films of bulk-WO_3 in ethanol and nano-WO_3 in water were fabricated by drop-coating the suspensions and drying in air. The electrolyte (aqueous 0.1 M H_2SO_4 at pH 1) was degassed with nitrogen for ten minutes prior to each measurement. The potential of the $[Fe(CN)_6]^{3-/4-}$ redox couple (+0.36 V vs NHE) was used to calibrate the system. Potentials were generated and currents observed with a Gamry Reference 600 potentiostat controlled by a PC. The water oxidation potential was measured by applying anodic scans (10 mV/s). Photocurrent onset potentials were determined by applying cathodic scans (10 mV/s) under chopped light. Illumination was provided by a 300 W Xe arc lamp, equipped with a water filter, using a SiO_2 fiber optics cable that delivered 120 ± 20 mW/cm^2 at the electrode, as measured with a GaAsP photodetector. Surface photovoltage measurements were conducted under vacuum (2×10^{-4} mBar) on nano-WO_3 films on F:SnO_2 (FTO) substrates. A gold Kelvin probe (Delta PHI Besocke) served as the reference electrode. Samples were illuminated with monochromatic light from a 150 W Xe-lamp filtered through a Oriel Cornerstone 130 monochromator (1−10 mW cm^{-2}).

Other Measurements. Diffuse reflectance UV−vis spectra were collected using an Ocean Optics DH2000 light source and HR2000 CG−UV−NIR spectrometer. Transmission electron microscopy (TEM) was performed using a Philips CM120 transmission electron microscope and a Gatan MegaScan digital camera. Bright field high resolution transmission electron microscopy (BF-HR-TEM) images were taken using a JEOL 2500SE 200 kV TEM. Z-contrast high angle annular dark field scanning TEM (HAADF-STEM) images were taken using a JEOL 2100F STEM with 200 kV field-emission gun and a spherical aberration corrector.

RESULTS AND DISCUSSION

The addition of tetrabutylammonium hydroxide to the suspension of WO_3 nanosheets during workup (Figure 2) improves product separation and provides access to pure WO_3 nanosheets on the gram scale, although at low yield (4.5% based on $Bi_2W_2O_9$). According to TEM (Figure 3A), these sheets are fully exfoliated and possess an average edge length of 90 (±38) nm. The homogeneous thickness of these sheets (0.75 nm, from unit cell parameters) is supported by the uniform contrast among separate particles. HAADF-STEM (Figure 3B) confirms the crystalline structure of these sheets. Interestingly, the angle between rows (97°) and their spacing (0.37 and 0.38 nm) is consistent with the (001) plane of the monoclinic WO_3 lattice with unit cell parameters a = 7.297 Å, b = 7.539 Å, c = 7.688 Å, and β = 90.85°.[15] The structure of the $Bi_2W_2O_9$ parent material (Figure 1), on the other hand, consists of WO layers (Figure 3C) with tetragonal symmetry. This is confirmed by the 90° angle between rows and their spacing (0.27 and 0.30 nm), which is consistent with the $(10\bar{3})$ plane in orthorhombic $Bi_2W_2O_9$, that is observed with HR-TEM (Figure 3D).

dx.doi.org/10.1021/cm203293j | Chem. Mater. 2012, 24, 698−704

Table 1. Oxygen Evolution Data For Bulk-WO_3 and Nano-WO_3

sample	conditions	initial/final pH	total O_2 generated (μmol)	O_2 generation rate, 1st hour (μmol/h)	quantum efficiency (%) at 375 nm	turnover no. (μmol O_2/ μmol tungsten)
$Bi_2W_2O_9$[a]	0.05 M Ag^+/UV (450 W Hg lamp) from Kudo et al.[21]			281		
bulk-WO_3[b]	8.3 mM Ag^+/>250 nm	4.96/2.22	133.9	69.7		0.621
nano-WO_3[b]	8.3 mM Ag^+/>250 nm	6.48/2.61	61.2	35.5		0.284
bulk-WO_3[b]	8.3 mM Ag^+/>400 nm	4.87/2.21	117.0	39.8		0.543
nano-WO_3[b]	8.3 mM Ag^+/>400 nm	6.50/2.71	31.8	5.2		0.147
bulk-WO_3[b]	2.1 mM Ce^{4+}/>400 nm	2.28/2.31	27.6	8.4		0.128
nano-WO_3[b]	2.1 mM Ce^{4+}/>400 nm	2.85/2.90	16.1	5.9		0.075
bulk-WO_3[c]	1.7 mM Ag^+/375 nm	6.35/3.71	10.5	2.5	1.43[d]	0.243
nano-WO_3[c]	1.7 mM Ag^+/375 nm	6.51/3.37	10.7	3.2	1.55[d]	0.248

[a]1 g. [b]50 mg. [c]10 mg. [d]Quantum efficiencies were determined under LED illumination at 375 nm with 10 mg of catalyst in a solution of 1.7 mM $AgNO_3$.

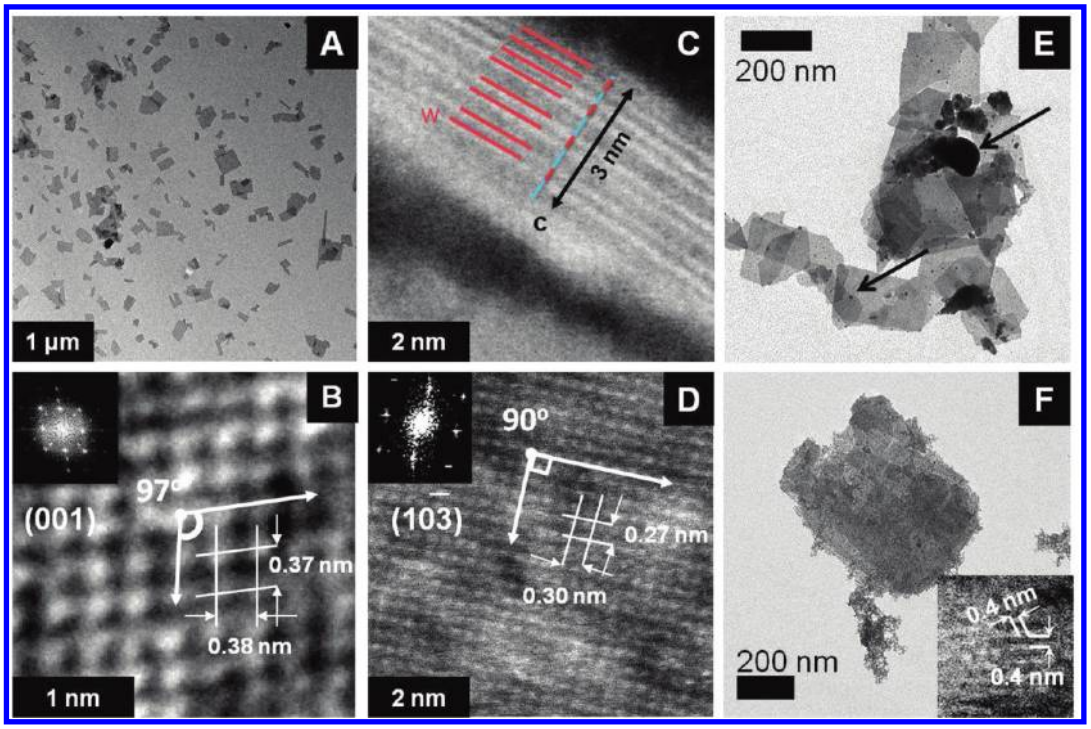

Figure 3. HR-TEM and HAADF-STEM images of nano-WO_3 (A, B) after exfoliation and $Bi_2W_2O_9$ (C, D) during exfoliation. Comparison of the observed lattice in images B and D reveals that a change from tetragonal in $Bi_2W_2O_9$ (D) to monoclinic in nano-WO_3 (B) has occurred. HR-TEM image (C) depicts a partially exfoliated $Bi_2W_2O_9$ crystal from the side, revealing WO_3 layers (indicated with red lines) separated by darker regions of partially removed $Bi_2O_2^{2+}$. Nano-WO_3 (E) after a 5 h irradiation in 8.3 mM $AgNO_3$ (photodeposited Ag^0 is indicated with arrows) and nano-WO_3 (F) after a 5 h irradiation (>400 nm) in 8.3 mM $(NH_4)_2Ce(NO_3)_6$. Inset: HR-TEM image of secondary WO_3 nanocrystal formed by Ostwald ripening.

The structure change is likely driven by an increase in packing density of W and O atoms. It appears to require basic conditions that are present during treatment with TMA(OH)/TBA(OH), since acid treatment of $Bi_2W_2O_9$ alone is known to preserve the tetragonal structure of the $H_2W_2O_7$ layers.[16] A full structure conversion to monoclinic WO_3 can be achieved by removing the nanosheets from solution, and drying them under elevated temperature (90 °C). Such samples show the X-ray diffraction pattern typical of monoclinic WO_3 (top of Figure 4, JCPDS 43−1035). Like the structure distortion above, this transformation leads to a reduction of surface energy, and an increase in packing density, which allows for greater lattice enthalpy.

Figure 5 compares diffuse reflectance optical spectra of nano-WO_3 with those of bulk-WO_3 and of $Bi_2W_2O_9$. The spectra are represented as the Kubelka−Munk function to reduce the scattering contribution from the powders. It can be seen that $Bi_2W_2O_9$ (2.81 eV) has an increased band gap compared to bulk-WO_3 (2.68 eV). The increase in band gap has to be at least partially attributed to quantum size confinement of the W_2O_6 layers in $Bi_2W_2O_9$. The layers are only 0.75 nm thick, below the Bohr exciton radius of metal oxide particles (e.g., for TiO_2, r_B = 0.75−1.9 nm).[17] Upon exfoliation to nano-WO_3, the band gap increases further to 2.88 eV. This is probably a result of the structure change to monoclinic, which allows for a less strained, more stable coordination environment around W. As a consequence, the HOMO−LUMO gap is expected to increase.

Surface photovoltage spectroscopy is a useful tool to probe generation and separation of charge carriers in semiconductor

dx.doi.org/10.1021/cm203293j | Chem. Mater. 2012, 24, 698−704

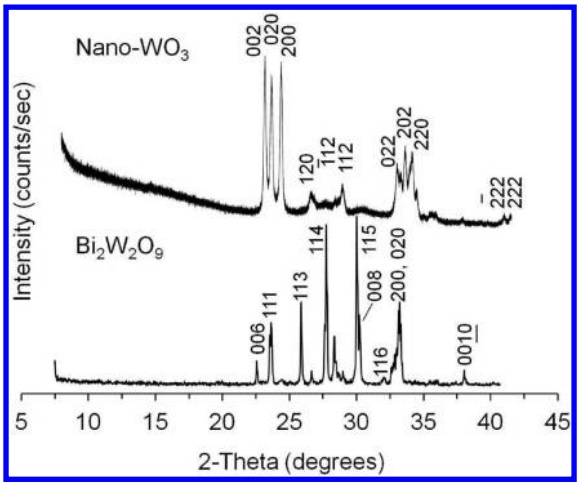

Figure 4. Powder X-ray diffraction (XRD) spectra of nano-WO_3 and the parent material $Bi_2W_2O_9$ (JCPDS No. 089−8114). nano-WO_3 is consistent with that of monoclinic WO_3 (JCPDS No. 43−1035).

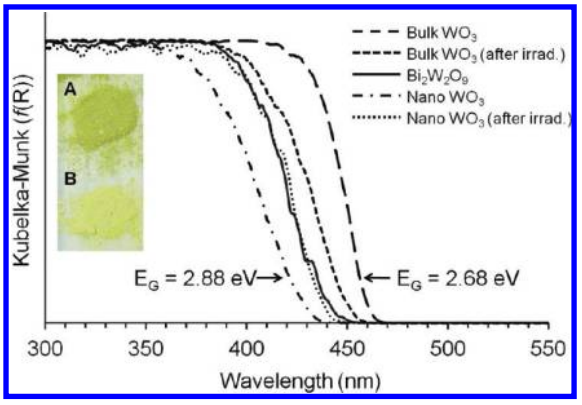

Figure 5. Diffuse reflectance spectra of bulk-WO_3 before and after visible (>400 nm) light irradiation for 22 h in a 44 mM $(NH_4)_2Ce(NO_3)_6$ solution. Spectra of the parent material $Bi_2W_2O_9$ and exfoliated nano-WO_3 before and after visible light irradiation for 5 h in a 21 mM $(NH_4)_2Ce(NO_3)_6$ solution. Inset: Photographs of bulk-WO_3 (A) before and (B) after irradiation.

nanoparticles.[12,18−20] Here, a nanocrystal film of nano-WO_3 was first deposited on gold or F:SnO_2 substrate and placed into a vacuum chamber at 2×10^{-4} mBar. A vibrating gold Kelvin probe is then used to measure the contact potential difference (CPD) of the sample versus the gold reference. In the dark the CPD values are determined mainly by the difference of work-functions between the sample and the reference probe. Under band gap illumination, photogenerated charge carriers change the CPD value. This is shown in Figure 6 as a function of illumination energy. A negative change of the CPD value occurs as the photon energy approaches the band gap of the material. The negative sign of ΔCPD indicates that photogenerated electrons are preferentially separated toward the FTO substrate, leaving the WO_3 surface increasingly positively charged. The ΔCPD value reaches its maximum value of −0.360 V at 3.5 eV. This demonstrates that nano-WO_3 is able to generate and separate electron−hole pairs under band gap excitation. The CPD signal of a fresh WO_3 film under repeated illumination is shown in Figure 6B. Initial exposure of the film to 50 s of 400 nm light leads to a 0.25 V drop in CPD. During the following 500 s dark period, the signal recovers only partially (35 mV), and subsequent illumination/dark cycles result in increasingly smaller ΔCPD signals. This indicates that the positive charges on the WO_3 film are located in deep trap sites that are not in thermal equilibrium with the FTO substrate. We tentatively identify these sites as the redox sites for water oxidation.

To evaluate the ability of the WO_3 nanosheets to photo-oxidize water, samples of nano- and bulk-WO_3 were suspended in aqueous $AgNO_3$ or $(NH_4)_2Ce(NO_3)_6$ and illuminated with a 300 W Xe arc lamp using its full (>250 nm) or filtered (>400 nm) spectrum. Experiments were carried out with limiting concentrations of sacrificial agents to avoid complications due to precipitation of the catalysts caused by high ionic strength and low pH. The results of these experiments are shown in Table 1 and Figure 7. It can be seen that the highest O_2 evolution rates (69.7 μmol h^{-1} for bulk and 35.5 μmol h^{-1} for nano-WO_3) are observed under >250 illumination in the presence of 8.3 mM Ag^+ (Figure 7A). After 5 h of irradiation, 100 and 59% of the possible total amount of O_2 have been evolved by bulk- and nano-WO_3, respectively. Under visible light (>400 nm), both materials are considerably less active (Figure 7B). Here, bulk- and nano-WO_3 support rates of 39.8 μmol h^{-1} and 5.2 μmol h^{-1} (with 50 mL of 8.3 mM Ag^+) respectively, which is about 1.8 (bulk) and 6.8 (nano) times less

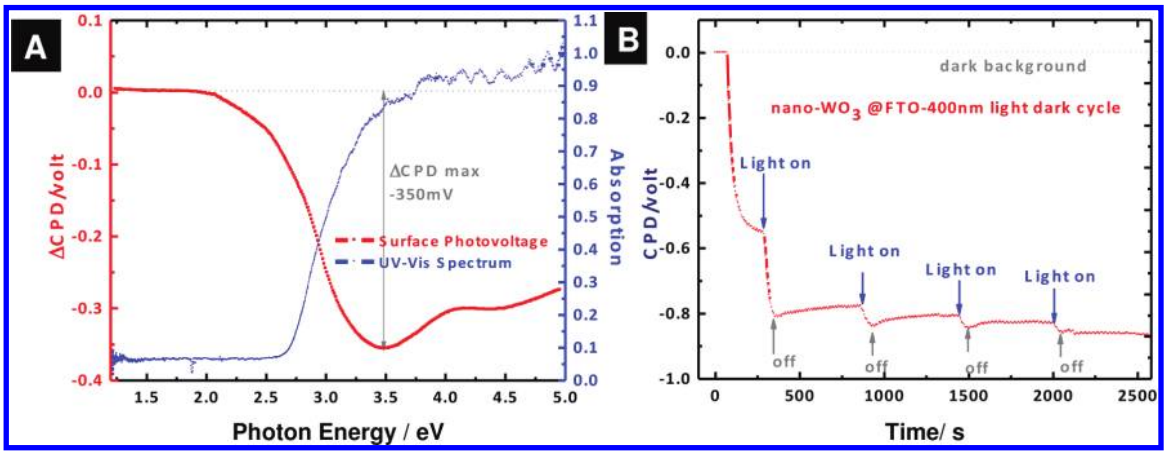

Figure 6. (A) Light-induced contact potential change ΔCPD (left axis) and absorption spectrum (right axis) of nano-WO_3 film on F:SnO_2 (FTO) electrode in vacuum (2×10^{-4} mbar) versus excitation energy. (B) ΔCPD signal for nano-WO_3 film on FTO substrate under repeated illumination at 400 nm.

dx.doi.org/10.1021/cm203293j | Chem. Mater. 2012, 24, 698−704

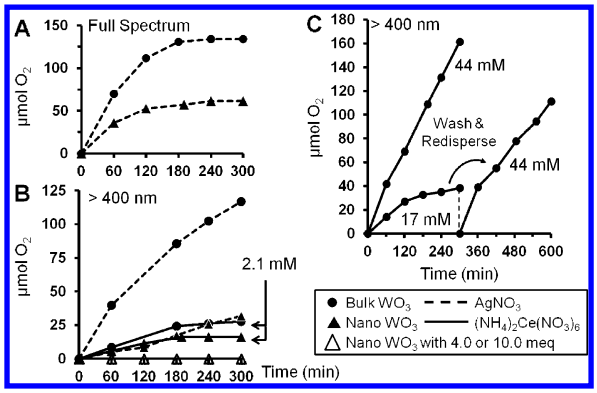

Figure 7. Oxygen evolution data under (A) full spectrum (>250 nm) irradiation and under (B) visible only (>400 nm) irradiation. Experiments were carried out in degassed/deionized water in the presence of 50 mL of 8.3 mM sacrificial electron acceptor (unless other indicated). (C) Comparison of oxygen evolution from visible irradiation of bulk-WO_3 for a single irradiation versus two sequential irradiations, which included washing and redispersion of the catalyst in new sacrificial acceptor solution.

than that under >250 nm irradiation. After 5 h of irradiation, 100% of the total possible O_2 (based on 415 μmol $AgNO_3$) was produced by bulk-WO_3. For nano-WO_3, 31% of all sacrificial reagent is consumed based on an observed total of 31.8 μmol O_2. To avoid complications from silver deposition, we repeated irradiations for the tungsten oxides with ammonium cerium nitrate. Because of UV instability, Ce^{4+} could only be used for visible light experiments. Interestingly, no O_2 was evolved from nano-WO_3 when 8.3 mM or 21 mM of Ce^{4+} were present (approximately 2 and 5 meq., respectively). However, with 2.1 mM Ce^{4+}, we observed O_2 formation at an initial rate of 5.9 μmol h^{-1}, somewhat above that with Ag^+ (5.2 μmol h^{-1}). After 5 h, a total of 16.1 μmol of O_2 has evolved, corresponding to a 61% consumption of the sacrificial donor. These results indicate that Ce^{4+} is not as good as silver in driving photochemical water oxidation. Summarizing these tests nano-WO_3 is not as efficient for photochemical O_2 production as bulk-WO_3. As the right column in Table 1 shows, neither bulk- nor nano-WO_3 reach a turnover number greater than unity. However, the picture changes when the experiments are repeated with Ag^+ under monochromatic irradiation at 375 nm. Here, bulk-WO_3 reaches an initial O_2 evolution rate of 2.5 μmol h^{-1}, compared to 3.2 μmol h^{-1} for nano-WO_3. Within the first hour, the apparent quantum efficiencies are 1.43% for bulk and 1.55% for the nanomaterial. These results indicate that nano-WO_3 is slightly more active than bulk-WO_3 and that the lesser performance of nano-WO_3 under Xe-light is due to its lower light absorption cross-section, caused by the larger band gap of 2.88 eV, compared to 2.68 eV for the bulk (Figure 5).

Over the course of the irradiations, the materials undergo several changes, which are responsible for the loss of O_2 activity over time. As the TEM for irradiated nano-WO_3 (Figure 3E) shows, photochemical oxygen evolution in the presence of $AgNO_3$ is accompanied by the formation of silver particles on the nano-WO_3 and in solution. The silver particles compete for photons and cover up redox active sites on WO_3, rendering the material less active. At the same time, water oxidation leads to release of protons and a decrease of the solution pH. During a typical 5 h irradiation (in 8.3 mM $AgNO_3$) the pH falls from an initial value of ~4.9 to a final value of ~2.0 for bulk-WO_3 and from 6.5 to 2.6 for nano-WO_3 (Table 1). This leads to aggregation of nano-WO_3 (Figure 3E), as the pH approaches the point of zero charge of the material. The aggregation problems are more severe with $(NH_4)_2Ce(NO_3)_6$ because of the acidity of ammonium ion.

Lastly, we note that irradiation with the Ce^{4+} salt does also lead to changes in the WO_3 materials. For postirradiated nano-WO_3, a red shift of the absorption edge from 430 to 440 nm is evident in the optical spectra (Figure 5). Inspection of the irradiated nano-WO_3 by TEM reveals ~5 nm nanoparticles near the original WO_3 nanosheets (Figure 3F). HR-TEM images (inset in Figure 3F) confirm that these particles are crystalline and energy dispersive spectroscopy indicates high amounts of tungsten and low amounts of cerium present on both the particulate matter surface and the original nano-WO_3 after irradiation in $(NH_4)_2Ce(NO_3)_6$ solution. We hypothesize that irradiation in the presence of Ce^{4+} salt promotes recrystallization of the nanosheets to form WO_3 nanodots with lower surface area (Ostwald ripening), and increased diameter (5 nm instead of 0.75 nm for the nanosheets). This size increase explains the red shift in the spectrum upon irradiation. The transformation of nano-WO_3 is facilitated by the ammonium ions in $(NH_4)_2Ce(NO_3)_6$ and likely involves the tungstate (WO_4^{2-})[22] and para tungstate ($W_{12}O_{42}^{4-}$) ions. This side reaction is the likely cause for the low photocatalytic activity in the presence of $(NH_4)_2Ce(NO_3)_6$.

Opposite to nano-WO_3, irradiation of bulk-WO_3 in the presence of the Ce^{4+} salt causes a small blue shift of the absorption spectrum from 462 to 453 nm (2.74 eV), and a concomitant change of the color from green to yellow (inset in Figure 5). These optical changes are related to the disappearance of surface impurities (reduced W ions) in the initial material.[23] The removal of these sites does not degrade the catalytic performance of the material. As Figure 7C shows, any loss of O_2 activity upon irradiation with 17 mM Ce^{4+} is temporary, and can be restored upon washing the material and redispersing it in a fresh solution of 50 mL of 44 mM Ce^{4+}.

In order to investigate the kinetics of water oxidation with both types of WO_3, electrochemical scans on films of the materials were performed in the dark using 0.1 M H_2SO_4 as electrolyte (Figure 8). Under these conditions, both nano- and bulk-WO_3 are found to oxidize water at +2.19 V (NHE, pH 1, 1.0 mA cm^{-2}), which is slightly improved over what Hodes et al. reported for WO_3 films in 1976 (2.2 V at 0.2 mA cm^{-2}, note the lower current density).[1] These electrochemical overpotentials for water oxidation are exceptionally high (nearly 1.0 V) in comparison to other materials, and may be viewed as a limiting factor in the use of WO_3 as a photoanode material.

Under illumination, small photocurrents (<1 μA cm^{-2}) can be observed for both nano- and bulk-WO_3. The small size of the current is due to the low quality of the films and bad electrical contact with the electrode. Photocurrent onsets are observed at potentials above +0.23 V for nano-WO_3, and +0.11 V for bulk-WO_3. These values can be taken to approximate the conduction band edge of WO_3. Considering that flatband potentials depend strongly on material preparation and pH,[24] the values compare favorably with the literature (0.33−0.6 V for WO_3 at pH 0,[1,25] and 0.20−0.25 V[24,26] at pH 2−4.68).

The photocurrent onset potentials and the optical band gap data can be used to construct the energy diagram in Figure 9. The diagram shows that the energetics of both materials are similar, except that the conduction and valence band edges of nano-WO_3 are shifted to more oxidizing potentials and that its band gap is slightly larger (2.88 eV instead of 2.74 eV). For both materials, oxidation of water and reduction of silver ion are

dx.doi.org/10.1021/cm203293j | Chem. Mater. 2012, 24, 698−704

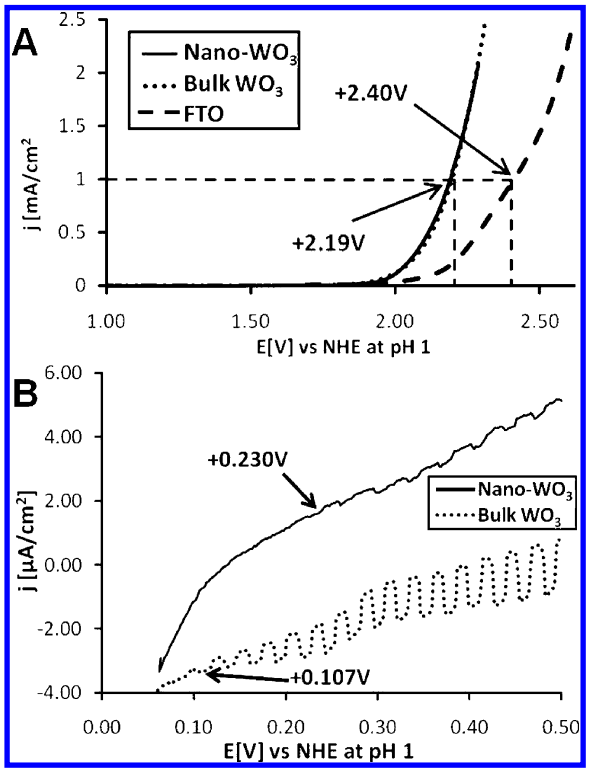

Figure 8. Electrochemical data for bulk- and nano-WO_3 films drop-coated onto FTO electrodes in 0.1 M H_2SO_4 solution. (A) Voltammetric traces (10 mV s^{-1}), and (B) photocurrent spectra (10 mV s^{-1}) under chopped irradiation (>250 nm). Potentials are reported against normal hydrogen electrode (NHE).

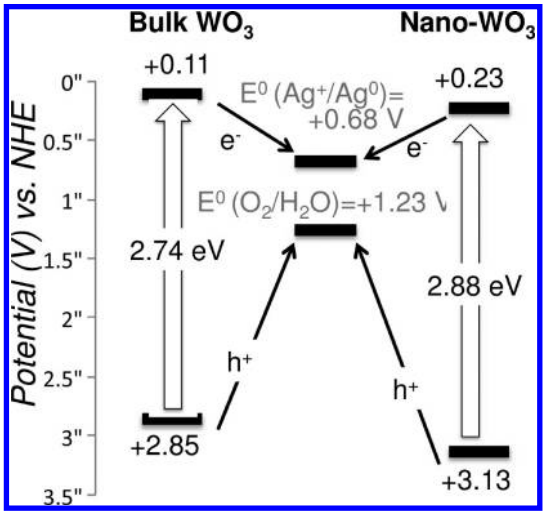

Figure 9. Energy diagram for photochemical water oxidation at pH 0 with bulk- and nano-WO_3. The Ag^+/Ag potential is for a 10 mM solution.

thermodynamically favorable. Significant energy loss (1.6–1.9 eV) occurs during hole transfer from the WO_3 valence band to water. However, approximating the oxidation barrier with the dark water oxidation overpotential (1.0 V, Figure 8A), this expense may be necessary to drive the reaction. The diagram also shows that both systems are theoretically capable of net conversion of photochemical into chemical energy (about 1.23–0.68 eV = 0.55 eV per photon), if one would increase the quantum efficiency of presently 1.5% to about unity.

CONCLUSION

In summary, we have demonstrated that the principle photophysical and photochemical properties of WO_3 are maintained in subnanometer thick single-crystal WO_3 nanosheets, and that the photochemical water oxidation efficiency of nano-WO_3 is comparable to that of the bulk form. Because of quantum size confinement, a blue shift of the photoresponse occurs in the nanomaterial. The principle limitations of nano-WO_3 for water oxidation arise from the use of silver ion as the electron acceptor (leads to silver deposits) and from the tendency of the nanosheets to aggregate (in the solid state) or recrystallize (Ostwald ripening) when in contact with solutions of ammonium cerium nitrate.

AUTHOR INFORMATION

Corresponding Author

*E-mail: fosterloh@ucdavis.edu. Fax: (+1)530 752 8995.

ACKNOWLEDGMENTS

F.E.O. thanks Thomas Dittrich (Helmholtz Center Berlin for Materials and Energy) for the introduction to surface photovoltage spectroscopy and for helpful discussions. M.R.W. thanks A.J.M. T.K.T. thanks NSF for a Graduate Research Fellowship 2011. Financial support was provided by Research Corporation for Science Advancement (Scialog award), by the National Science Foundation (NSF, Grants 0829142 and 1133099) and by the U.S. Department of Energy under Grant FG02-03ER46057.

REFERENCES

(1) Hodes, G.; Cahen, D.; Manassen, J. *Nature* **1976**, *260*, 312.
(2) Hardee, K. L.; Bard, A. J. *J. Electrochem. Soc.* **1977**, *124*, 215.
(3) Darwent, J. R.; Mills, A. *J. Chem. Soc., Faraday Trans. II* **1982**, *78*, 359.
(4) Wang, H. L.; Deutsch, T.; Turner, J. A. *J. Electrochem. Soc.* **2008**, *155*, F91.
(5) Sasaki, Y.; Nemoto, H.; Saito, K.; Kudo, A. *J. Phys. Chem. C* **2009**, *113*, 17536.
(6) Kato, H.; Sasaki, Y.; Wase, A.; Kudo, A. *B. Chem. Soc. Jpn.* **2007**, *80*, 2457.
(7) Abe, R.; Takata, T.; Sugihara, H.; Domen, K. *Chem. Commun.* **2005**, *30*, 3829.
(8) Higashi, M.; Abe, R.; Teramura, K.; Takata, T.; Ohtani, B.; Domen, K. *Chem. Phys. Lett.* **2008**, *452*, 120.
(9) Maeda, K.; Higashi, M.; Lu, D. L.; Abe, R.; Domen, K. *J. Am. Chem. Soc.* **2010**, *132*, 5858.
(10) Higashi, M.; Abe, R.; Takata, T.; Domen, K. *Chem. Mater.* **2009**, *21*, 1543.
(11) Townsend, T. K.; Sabio, E. M.; Browning, N. D.; Osterloh, F. E. *Energy Environ. Sci.* **2011**, *4*, 4270.
(12) Frame, F. A.; Townsend, T. K.; Chamousis, R. L.; Sabio, E. M.; Dittrich, T.; Browning, N. D.; Osterloh, F. E. *J. Am. Chem. Soc.* **2011**, *133*, 7264.
(13) Tanaka, D.; Oaki, Y.; Imai, H. *Chem. Commun.* **2010**, *46*, 5286.
(14) Schaak, R. E.; Mallouk, T. E. *Chem. Commun.* **2002**, *7*, 706.
(15) Loopstra, B. O.; Boldrini, P. *Acta Crystallogr.* **1966**, *21*, 158.
(16) Kudo, M.; Ohkawa, H.; Sugimoto, W.; Kumada, N.; Liu, Z.; Terasaki, O.; Sugahara, Y. *Inorg. Chem.* **2003**, *42*, 4479.
(17) Sant, P. A.; Kamat, P. V. *Phys. Chem. Chem. Phys.* **2002**, *4*, 198.
(18) Gross, D.; Mora-Seròl, I. n.; Dittrich, T.; Belaidi, A.; Mauser, C.; Houtepen, A. J.; Como, E. D.; Rogach, A. L.; Feldmann, J. *J. Am. Chem. Soc.* **2010**, *132*, 5981.
(19) Mora-Sero, I.; Bisquert, J.; Dittrich, T.; Belaidi, A.; Susha, A. S.; Rogach, A. L. *J. Phys. Chem. C* **2007**, *111*, 14889.

(20) Beranek, R.; Neumann, B.; Sakthivel, S.; Janczarek, M.; Dittrich, T.; Tributsch, H.; Kisch, H. *Chem. Phys.* **2007**, *339*, 11.
(21) Kudo, A.; Hijii, S. *Chem. Lett.* **1999**, *28*, 1103.
(22) Lillard, R. S.; Kanner, G. S.; Butt, D. P. *J. Electrochem. Soc.* **1998**, *145*, 2718.
(23) Chatten, R.; Chadwick, A. V.; Rougier, A.; Lindan, P. J. D. *J. Phys. Chem. B* **2005**, *109*, 3146.
(24) Diquarto, F.; Dipaola, A.; Sunseri, C. *Electrochim. Acta* **1981**, *26*, 1177.
(25) Leland, J. K.; Bard, A. J. *J. Phys. Chem.* **1987**, *91*, 5083.
(26) Wang, H. L.; Lindgren, T.; He, J. J.; Hagfeldt, A.; Lindquist, S. E. *J. Phys. Chem. B* **2000**, *104*, 5686.